NUCLEAR SCIENCE AND ENGINEERING: 64, 563-575 (1977)

A Finite Element Depletion Diffusion Calculation Method with Space-Dependent Cross Sections

Alain Kavenoky and Jean-Jacques Lautard

Centre d'Etudes Nucléaires de Saclay
Service d'Etudes des Réacteurs et de Mathématiques Appliquées
B.P. No. 2, 91190 Gif-sur-Yvette, France

Received January 21, 1977
Revised April 5, 1977

A new solution method for the diffusion depletion equation is presented. Space-dependent macroscopic cross sections are represented in the framework of a finite element basis, and the finite element method is extended to deal with these space-dependent cross sections. This method has been implemented in the NEPTUNE system of reactor calculation to be applied to two- and three-dimensional depletion calculation of large reactors. Numerical calculations are presented, and comparisons are performed with standard methods.

I. INTRODUCTION

From a theoretical point of view, the solution of the diffusion equation can be obtained using any numerical method: finite differences, finite elements, or nodal synthesis. These methods can be used efficiently for the treatment of a new core with piecewise constant cross sections; the finite element method can save a large part of the computing time by comparison to the finite difference method. This result is obtained using large elements and therefore reducing the number of unknowns.

In the case of a depleted core, the cross sections are space dependent, and the mesh size is limited by the variations of the cross sections. The finite difference up to now has been the only method to be used in this case for accurate calculations.

In this paper, a new solution method for the diffusion depletion equation is presented. The space-dependent macroscopic cross sections are treated in the framework of a finite element basis, and the solution method is extended to deal with these space-dependent cross sections. This calculation method is applied for two- and three-dimensional depletion calculation of large reactors.

The extension of the finite element method to deal with space-dependent cross sections is presented in Sec. II; the method used for accounting for depletion dependent cross sections is developed in Sec. III. A new extension of this method is presented in Sec. IV; it accounts for a complete treatment of any fission product decay chain and buildup of heavy isotopes. Numerical results obtained using this method are compared with standard ones in Sec. V.

II. A FINITE ELEMENT DIFFUSION CALCULATION FOR SPACE-DEPENDENT CROSS SECTIONS

Diffusion calculations using the finite element method have been published.[1] Here, a brief presentation is given to show the differences in the calculation due to space-dependent cross sections.

The three-dimensional diffusion equation is considered in the multigroup approximation:

$$\text{div}\left[D^g(\boldsymbol{r})\ \text{grad}\ \Phi^g(\boldsymbol{r})\right] - \Sigma_a^g(\boldsymbol{r})\Phi^g(\boldsymbol{r}) + S^g(\boldsymbol{r}) = 0 \quad . \quad (1)$$

[1]CHANG-MU-KANG and K. F. HANSEN, "Finite Element Methods for Space Time Reactor Analysis," MIT 3903-5, MITNE-135, Massachusetts Institute of Technology (November 1971).

Here,

$D^g(\mathbf{r})$ = diffusion coefficient in group g

$\Sigma_a^g(\mathbf{r})$ = total absorption cross section in group g

$S^g(\mathbf{r})$ = source term due to fission, slowing down, and thermalization.

This equation is valid for a reactor Ω; on the boundary $\Gamma = \partial\Omega$, the boundary conditions are

$$\mathbf{r} \in \Gamma_1 \quad \Phi^g(\mathbf{r}) = 0$$

$$\mathbf{r} \in \Gamma_2 \quad D^g(\mathbf{r}) \frac{\partial}{\partial n} \Phi^g(\mathbf{r}) + \gamma^g(\mathbf{r}) \Phi^g(\mathbf{r}) = 0 \quad , \qquad (2)$$

with the conditions

$$\Gamma = \Gamma_1 \cup \Gamma_2$$

and

$$\Gamma_1 \cap \Gamma_2 = \phi \quad .$$

Let us define the linear functional $F^g(\psi)$:

$$F^g(\psi) = -\int_\Omega \Psi(\mathbf{r}) S^g(\mathbf{r}) d\mathbf{r} \quad .$$

By use of the Kourganoff's functional,[2] a variational representation of $F^g(\psi)$ is given by

$$F^g(\psi) = \int_\Omega \Sigma_a^g(\mathbf{r}) \Psi(\mathbf{r})^2 d\mathbf{r} - \int_\Omega \Psi(\mathbf{r}) \operatorname{div}[D^g(\mathbf{r}) \operatorname{grad} \psi(\mathbf{r})] d\mathbf{r} - 2\int_\Omega S^g(\mathbf{r}) \psi(\mathbf{r}) d\mathbf{r} \quad .$$

By an integration by parts, it is transformed into

$$F^g(\psi) = \int_\Omega D^g(\mathbf{r}) |\operatorname{grad} \Psi(\mathbf{r})|^2 d\mathbf{r} + \int_\Omega \Sigma_a^g(\mathbf{r}) \psi^2(\mathbf{r}) d\mathbf{r} - 2\int_\Omega S^g(\mathbf{r}) \psi(\mathbf{r}) d\mathbf{r} + \int_{\Gamma_2} \gamma^g(\mathbf{r}) \psi^2(\mathbf{r}) d\mathbf{r} \quad . \qquad (3)$$

The minimization of the functional of Eq. (3) in the space V,

$$V = \left[\psi \,|\, \psi \in L^2(\Omega);\ \frac{\partial \psi}{\partial x_i} \in L^2(\Omega);\ \psi(\mathbf{r}) = 0 \quad \mathbf{r} \in \Gamma_1 \right] ,$$

constitutes the variational form of the diffusion equation, Eq. (1) The Ritz-Galerkin method uses this form of the equation.

The minimization of the functional is performed on the subset V_h of V, the dimension of which is N. This subset V_h is generated by the basis

$$V_h = [\, W_1(\mathbf{r}) \ldots W_n(\mathbf{r}) \,] \quad ,$$

and therefore the expansion of ψ is

$$\psi_h(\mathbf{r}) = \sum_{i=1}^{i=N} \alpha_i W_i(\mathbf{r}) \quad . \qquad (4)$$

[2]V. KOURGANOFF, *Ann Astrophys.*, **12**, 169 (1949).

The minimum condition leads to a system of linear equations:

$$A^g \alpha = f^g \quad , \qquad (5)$$

where

$$A_{ij}^g = \int_\Omega D^g(\mathbf{r}) \operatorname{grad} W_i(\mathbf{r}) \cdot \operatorname{grad} W_j(\mathbf{r}) d\mathbf{r} + \int_\Omega \Sigma_a^g(\mathbf{r}) W_i(\mathbf{r}) W_j(\mathbf{r}) d\mathbf{r} + \int_{\Gamma_2} \gamma^g(\mathbf{r}) W_i W_j \, d\mathbf{r}$$

$$f_i^g = \int_\Omega S^g(\mathbf{r}) W_i(\mathbf{r}) d\mathbf{r} \quad . \qquad (6)$$

II.A. Finite Element Method

This method is a special case of the Galerkin method: The $W_i(\mathbf{r})$ functions are chosen as piecewise polynomials continuous on Ω. For practical light water reactor calculations, rectangular parallelepiped elements have been chosen in the BILAN and TRIDENT modules of NEPTUNE (Refs. 3 and 4). The domain Ω is divided into n elements E_e satisfying the relations

$$\bigcup_{e=1}^{e=n} E_e = \Omega \qquad E_e \cap E_f = \phi \qquad e \neq f \quad .$$

Using these elements, two bases are defined, one for the representation of the fluxes and one for the representation of the cross sections.

II.B. Representation of the Fluxes

In the set of elements being chosen, nodes are chosen according to the order of the polynomial basis to be used; they may be inside the element, on a face of the element (in three-dimensional geometry), on an edge, or at a vertex. All these nodes are numbered, a node is marked by an index i, and a $W_i(\mathbf{r})$ function is associated with it.

Generally, the $W_i(\mathbf{r})$ are piecewise polynomials of order n_x in x, n_y in y, and n_z in z, defined on one or several elements depending on the node.

Case 1. The node i is inside the element E_e. The $W_i(\mathbf{r})$ function is a polynomial defined on the element E_e; the value of $W_i(\mathbf{r})$ is unity at node i and zero at all the other nodes of the element.

Case 2. The node i is on the face between elements E_e and E_f in three dimensions. The $W_i(\mathbf{r})$ function is made up of two polynomials, one

[3]A. KAVENOKY, "NEPTUNE: A Modular Scheme for the Calculation of Light Water Reactors," *Proc. Conf. Computational Methods in Nuclear Engineering*, Charleston, South Carolina, April 15-17, 1975, CONF-750413, Vol. II, p. V-27, Savannah River Laboratory (1975).

[4]J. BOUCHARD, A. KAVENOKY, and P. REUSS, *Trans. Am. Nucl. Soc.*, **20**, 365 (1975).

defined on element E_e and the other defined on element E_f. Each of these polynomials is defined to have a value of unity at node i and zero at the other nodes of the element.

Case 3. The node i is on an edge. The edge is shared by two elements in two-dimensional geometries and by four elements in three-dimensional geometries; $W_i(\boldsymbol{r})$ is formed by two and four polynomials, respectively, with the same definitions as in Case 2.

Case 4. The node i is on a vertex. The node is shared by four elements in two-dimensional geometries and by eight elements in three-dimensional geometries; $W_i(\boldsymbol{r})$ is formed by four and eight polynomials, respectively.

The flux is expanded over this basis according to Eq. (4); a change of indices may be performed. Let $\Upsilon_e(\boldsymbol{r})$ be the characteristic function of element E_e and define $Q_e^k(\boldsymbol{r})$ functions by

$$Q_e^k(\boldsymbol{r}) \equiv \Upsilon_e(\boldsymbol{r}) W_i(\boldsymbol{r}) \quad .$$

Here, $Q_e^k(\boldsymbol{r})$ is a polynomial defined on element E_e. (We have omitted for brevity details concerning the somewhat complex relationship between i and k.) It is easily shown that the expansion of Eq. (4) is equivalent to

$$\boldsymbol{r} \in E_e \qquad \psi_h(\boldsymbol{r}) = \sum_{k=1}^{k=P} \psi_e^k Q_e^k(\boldsymbol{r}) \quad , \tag{7}$$

where P is the number of nodes per element.

II.C. Representation of the Cross Section

A second basis is defined over the E_e elements. It is generated by polynomials $\Pi_e^l(\boldsymbol{r})$, which are defined only on the elements E_e, and its order is q. The diffusion coefficient and the macroscopic cross sections for any reaction r and any group g are represented by

$$\boldsymbol{r} \in E_e \qquad \Sigma_{re}^g(\boldsymbol{r}) = \sum_{l=1}^{l=q} \Sigma_{re}^g \Pi_e^l(\boldsymbol{r}) \quad ,$$

or by the equivalent relation,

$$\Sigma_r^g(\boldsymbol{r}) = \sum_{e=1}^{e=n} \sum_{l=1}^{l=q} \Sigma_{re}^{gl} \Pi_e^l(\boldsymbol{r}) \Upsilon_e(\boldsymbol{r}) \quad . \tag{8}$$

This expansion is not continuous across the boundary of an element.

II.D. Calculation of the Matrix Elements

Using the expansion of the flux [Eq. (4)] and of the cross sections [Eq. (8)], the matrix elements of Eq. (6) are now represented by the expansion:

$$A_{ij}^g = \sum_{e=1}^{e=n} \sum_{l=1}^{l=q} [D_e^{gl} B_{ij}^{el} + \Sigma_{ae}^{gl} C_{ij}^{el}] - E_{ij}^g \tag{9}$$

$$B_{ij}^{el} = \int_{E_e} \text{grad } W_i(\boldsymbol{r}) \cdot \text{grad } W_j(\boldsymbol{r}) \Pi_e^l(\boldsymbol{r}) d\boldsymbol{r} \tag{10}$$

$$C_{ij}^{el} = \int_{E_e} W_i(\boldsymbol{r}) W_j(\boldsymbol{r}) \Pi_e^l(\boldsymbol{r}) d\boldsymbol{r} \tag{11}$$

$$E_{ij} = \int_{\Gamma_2 \cap E_e} \gamma^g(\boldsymbol{r}) W_i(\boldsymbol{r}) W_j(\boldsymbol{r}) d\boldsymbol{r} \quad . \tag{12}$$

Comparing the set of Eqs. (9) through (12) to usual finite element formulas, the only difference comes from the $\Pi_e^l(\boldsymbol{r})$ terms that account for space-dependent cross sections. The calculation of the matrix is therefore more expensive than the usual method, but the calculations needed for the solution are the same as for the standard case.

II.E. Resolution of the Linear System of Equations

Equation (1) is an inhomogeneous diffusion equation for group g, and Eq. (5) is an inhomogeneous system of linear equations; three algorithms can be used for its solution:

1. The point successive over-relaxation (SOR) is used for large two- and three-dimensional problems that do not show a convergence problem.
2. The direct solution method LDL^T is used for standard-size two-dimensional problems, providing a fast and accurate solution.
3. The block SOR method is used for difficult three-dimensional calculations; in each plane, the direct solution 2 is performed, and the SOR method is applied to z calculations.

For the eigenvalue calculations, an outer iteration scheme is required. Usually, the Tchebychev method is used and, moreover, a special coarse-mesh rebalancing technique routine can be used.

III. A FINITE ELEMENT DEPLETION CALCULATION

In this section, we deal with macroscopic cross sections depending only on the burnup. The extension to a general depletion calculation is presented in Sec. IV.

Let us assume that, at a fixed time during the core life, the burnup can be represented by

$$\boldsymbol{r} \in E_e \qquad \tau_e(\boldsymbol{r}) = \sum_{l=1}^{l=q} \tau_e^l \Pi_e^l(\boldsymbol{r}) \quad . \tag{13}$$

Inside the element E_e, the bounds of $\tau_e(\boldsymbol{r})$ are defined by

$$\tau_e^1 = \min[\tau_e(\boldsymbol{r}) \mid \boldsymbol{r} \in E_e]$$

$$\tau_e^2 = \max[\tau_e(\boldsymbol{r}) \mid \boldsymbol{r} \in E_e] \quad .$$

At this point, a new assumption is added for τ, satisfying

$$\tau_e^1 \leq \tau \leq \tau_e^2 \quad .$$

The cross sections of all the reactions and all the groups vary linearly with τ:

$$\Sigma_{re}^g(\tau) = \Sigma_{re}^{g(1)} + \tau \Sigma_{re}^{g(2)} \quad .$$

The burnup-dependent cross sections are represented over the element E_e by

$$\Sigma_{re}^g(\boldsymbol{r}) = \Sigma_{re}^{g(1)} + \Sigma_{re}^{g(2)} \sum_{l=1}^{l=q} \tau_e^l \Pi_e^l(\boldsymbol{r}) \quad .$$

Now, the constant $\Sigma_{re}^{g(1)}$ is expanded over the Π_e^l basis,

$$\Sigma_{re}^{g(1)} = \sum_{l=1}^{l=q} \Sigma_{re}^{gl(1)} \Pi_e^l(\boldsymbol{r}) \quad ,$$

and we obtain

$$\Sigma_{re}^g(\boldsymbol{r}) = \sum_{l=1}^{l=q} \Sigma_{re}^{gl} \Pi_e^l(\boldsymbol{r}) \quad ,$$

with

$$\Sigma_{re}^{gl} = \Sigma_{re}^{gl(1)} + \tau_e^l \Sigma_{re}^{g(2)} \quad .$$

Using the assumption of the linear variation of cross section with burnup, the finite element expansion of the cross section has been obtained.

The last point to be proven is that the representation of the burnup is the same after a depletion step. Using the finite element solution of diffusion equation presented in Sec. II, the fluxes are represented by Eq. (7), and the power distribution $P(\boldsymbol{r})$ can be defined by

$$\boldsymbol{r} \in E_e \qquad P_e(\boldsymbol{r}) = \sum_{g=1}^{g=N} \sum_{k=1}^{k=P} K\Sigma_f^g(\boldsymbol{r}) \varphi_e^{gk} Q_e^k(\boldsymbol{r}) \quad .$$

In this expression, $K\Sigma_f^g(\boldsymbol{r})$ is the energy production cross section. It is represented by the usual expansion, which gives

$$\boldsymbol{r} \in E_e \qquad P_e(\boldsymbol{r}) = \sum_{l=1}^{l=q} \Pi_e^l(\boldsymbol{r}) \sum_{k=1}^{k=P} Q_e^k(\boldsymbol{r}) \sum_{g=1}^{g=N} K\Sigma_{fe}^{gl} \varphi_e^{gk} \quad . \tag{14}$$

This direct representation of $P_e(\boldsymbol{r})$ is not an expansion over the usual basis; using a minimization technique in L^2, an approximation of $P_e(\boldsymbol{r})$ will be obtained on the basis.

A formal expansion of $\tilde{P}_e(\boldsymbol{r})$ may be

$$\boldsymbol{r} \in E_e \qquad \tilde{P}_e(\boldsymbol{r}) = \sum_{l=1}^{l=q} P_e^l \Pi_e^l(\boldsymbol{r}) \quad . \tag{15}$$

The best approximation of $P_i(\boldsymbol{r})$ will be obtained using the least-squares method; the L^2 norm is used:

$$\| P_e - \tilde{P}_e \|^2 = \int_{E_e} [P_e(\boldsymbol{r}) - \tilde{P}_e(\boldsymbol{r})]^2 d\boldsymbol{r} \quad .$$

Using the definition of K_e^{kl}, Eqs. (14) and (15) provide

$$K_e^{kl} = \sum_{g=1}^{g=N} K\Sigma_{fe}^{gl} \varphi_e^{gk}$$

$$E(\tilde{P}_e) = \| P_e - \tilde{P}_e \|^2$$

$$= \int_{E_e} \left\{ \sum_{l=1}^{l=q} \Pi_e^l(\boldsymbol{r}) \left[P_e^l - \sum_{k=1}^{k=p} K_e^{kl} Q_e^k(\boldsymbol{r}) \right] \right\}^2 d\boldsymbol{r} \quad .$$

The stationarity condition leads to the system of linear equation:

$$\frac{\partial}{\partial P_e^m} E(\tilde{P}_e) = 0 \quad , \qquad m = 1 \text{ to } q$$

$$\frac{\partial}{\partial P_e^m} E(\tilde{P}_e) = 2 \int_{E_e} d\boldsymbol{r} \Pi_e^m(\boldsymbol{r}) \sum_{l=1}^{l=q} \Pi_e^l(\boldsymbol{r}) \times \left[P_e^l - \sum_{k=1}^{k=P} K_e^{kl} Q_e^k(\boldsymbol{r}) \right] \quad .$$

Finally,

$$\sum_{l=1}^{l=q} P_e^l \int_{E_e} \Pi_e^m(\boldsymbol{r}) \Pi_e^l(\boldsymbol{r}) d\boldsymbol{r} = \sum_{l=1}^{l=q} \sum_{k=1}^{k=P} K_e^{kl} \int_{E_e} \Pi_e^m(\boldsymbol{r}) \Pi_e^l(\boldsymbol{r}) Q_e^k(\boldsymbol{r}) d\boldsymbol{r} \quad , \qquad m = 1 \text{ to } q \quad . \tag{16}$$

This system of linear equations is solved for P_e^l.

Assuming a steady power distribution during a burnup step of time T, the added burnup at point $\boldsymbol{r}$ will be approximated by

$$\delta\tau_e(\boldsymbol{r}) = \frac{\tilde{P}_e(\boldsymbol{r}) T}{\rho(\boldsymbol{r})} \quad ,$$

where $\rho(\boldsymbol{r})$ is the density of the considered fuel. The total burnup will be

$$\tau_e^T(\boldsymbol{r}) = \sum_{l=1}^{l=q} \Pi_e^l(\boldsymbol{r}) \left(\tau_e^l + \frac{P_e^l T}{\rho} \right) \quad .$$

Therefore, it has been proven, with the assumption of the linear representation of the cross sections and the least-squares approximation of the power density, that the burnup distribution of Eq. (13) is valid during the depletion process.

IV. DETAILED TREATMENT OF THE DEPLETION PROCESS

In the previous section, the finite element method was extended to the treatment of space-dependent cross sections depending on the burnup. Now the total macroscopic cross section is represented by

$$\Sigma_{re}^g(\boldsymbol{r}) = \hat{\Sigma}_{re}^g(\boldsymbol{r}) + \sum_i C_e^i(\boldsymbol{r}) \sigma_{re}^{gi}(\boldsymbol{r}) \quad , \tag{17}$$

where $\hat{\Sigma}_{re}^g(\boldsymbol{r})$ is a partial macroscopic cross section treated as in Sec. III and C_e^i the density

the isotope i and $\sigma_{re}^{gi}(\boldsymbol{r})$, the corresponding microscopic cross sections.

To simplify the treatment, a few approximations are added.

1. At time T, the density $C_e^i(\boldsymbol{r})$ is expanded over the $\Pi_e^l(\boldsymbol{r})$ basis.
2. The microscopic cross sections $\sigma_{re}^{gi}(\boldsymbol{r})$ are assumed to depend on the burnup in the same way as the macroscopic cross sections:

$$\boldsymbol{r} \in E_e \qquad C_e^i(\boldsymbol{r}) = \sum_{l=1}^{q} C_e^{il}\,\Pi_e^l(\boldsymbol{r})$$

$$\sigma_{re}^{gi}(\boldsymbol{r}) = \sum_{l=1}^{q} \sigma_{re}^{gil}\,\Pi_e^l(\boldsymbol{r}) \quad .$$

The part of the macroscopic cross sections due to the separated isotopes is

$$\bar{\Sigma}_{re}^{g}(\boldsymbol{r}) = \sum_{i=1}^{i=n}\sum_{l=1}^{l=q}\sum_{m=1}^{m=q} C_e^{il}\,\sigma_{re}^{gim}\,\Pi_e^m(\boldsymbol{r})\Pi_e^l(\boldsymbol{r}) \quad .$$

Using the same minimization technique as in Sec. III for the power density, $\bar{\Sigma}_{re}^{g}(\boldsymbol{r})$ can be approximated by

$$\bar{\Sigma}_{re}^{g}(\boldsymbol{r}) = \sum_{l=1}^{l=q} \bar{\Sigma}_{re}^{gl}\Pi_e^l(\boldsymbol{r}) \quad .$$

Therefore, the total macroscopic cross section is represented on the basis previously used.

The differential equation for the density of isotope i can be written as

$$\frac{d}{dt}C_e^i(\boldsymbol{r},t) = -[\lambda^i + \sigma_a^i(\boldsymbol{r})\Phi(\boldsymbol{r})]C_e^i(\boldsymbol{r},t) + S_e^i(\boldsymbol{r},t) \quad , \tag{18}$$

where λ^i is the radioactive decay constant of isotope i and $S_e^i(\boldsymbol{r},t)$ is a source term due to decay, radiative capture, or fission yield.

Assuming a given concentration $C_e^i(\boldsymbol{r},0)$, the solution of this equation is

$$C_e^i(\boldsymbol{r},t) = C_e^i(\boldsymbol{r},0)\exp\{-t[\lambda^i + \sigma_{ae}^i(\boldsymbol{r})\Phi(\boldsymbol{r})]\} + \int_0^t S_e^i(\boldsymbol{r},t)\exp\{-[\lambda^i + \sigma_a^i(\boldsymbol{r})\Phi(\boldsymbol{r})](t-t')\}dt' \quad . \tag{19}$$

First, the exponential term is transformed. The average value of the absorption term is calculated on the E_e element:

$$\overline{\sigma_a\Phi_e} = \frac{1}{V_e}\int_{E_e}\sigma_{ae}^i(\boldsymbol{r})\Phi(\boldsymbol{r})d\boldsymbol{r} \quad .$$

This value is introduced in Eq. (19):

$$E(\boldsymbol{r}) = \exp\{-t[\lambda^i + \sigma_{ae}^i(\boldsymbol{r})\Phi(\boldsymbol{r})]\} = \exp[-t(\lambda^i + \overline{\sigma_a\phi_e})]\exp\{-t[\sigma_{ae}^i(\boldsymbol{r})\Phi(\boldsymbol{r}) - \overline{\sigma_a\Phi_e}]\} \quad .$$

The argument of the last exponential is assumed to be small, and a first-order expansion is taken:

$$E(\boldsymbol{r}) \simeq \exp[-t(\lambda^i + \overline{\sigma_a\phi_e})]\cdot\{1 - t[\sigma_{ae}^i(\boldsymbol{r})\Phi(\boldsymbol{r}) - \overline{\sigma_a\Phi_e}]\} \quad .$$

The usual expansion is assumed for $C_e^i(\boldsymbol{r},0)$ and $S_e^i(\boldsymbol{r},t)$:

$$C_e^i(\boldsymbol{r},0) = \sum_{l=1}^{l=q} C_{e0}^{il}\Pi_e^l(\boldsymbol{r})$$

$$S_e^i(\boldsymbol{r},t) = \sum_{l=1}^{l=q} S_e^{il}(t)\Pi_e^l(\boldsymbol{r}) \quad .$$

The density of isotope i becomes

$$C_e^i(\boldsymbol{r},t) = \exp[-t(\lambda^i + \overline{\sigma_a\phi_e})]\cdot\{1 - t[\sigma_{ae}^i(\boldsymbol{r})\Phi(\boldsymbol{r}) - \overline{\sigma_a\phi_e}]\} \times\left[\sum_{l=1}^{l=q} C_{e0}^{il}\Pi_e^l(\boldsymbol{r})\right] + \sum_{l=1}^{l=q}\Pi_e^l(\boldsymbol{r})\int_0^t S_e^{0l}(t') \times\exp[-(t-t')(\lambda^i + \overline{\sigma_a\phi_e})] \times\{1 - (t-t')[\sigma_{ae}^i(\boldsymbol{r})\Phi(\boldsymbol{r}) - \overline{\sigma_a\phi_e})]\}dt' \quad . \tag{20}$$

Finally, with one more use of the minimization technique, an approximation of C_e^i on the usual basis is determined. Thus, with the use of a few approximations, it has been shown that a density distribution expanded on finite element basis can be used for a depletion calculation.

V. NUMERICAL CALCULATIONS

V.A. Implementation of the Method

The method presented in Secs. II and III has been introduced in the ELECTRE module of NEPTUNE (Refs. 3 and 4). Two- and three-dimensional calculation capabilities are available, and a choice between several bases is offered for the flux representation $[Q_e^k(\boldsymbol{r})]$ and for the cross-section representation (Π_e^l).

V.A.1. Flux Representation

In two-dimensional calculations, four types of elements have been introduced: linear (4 nodes), parabolic (8 nodes), standard cubic (12 nodes), and Lagrangian cubic (16 nodes).

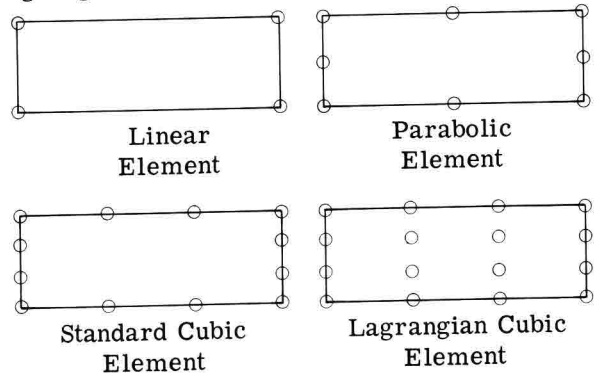

In three-dimensional calculations, the basis is obtained using the two-dimensional elements just described and an interpolation scheme in z. At present, this interpolation scheme may be linear or parabolic.

V.A.2. Cross-Section Representation

At the present time, linear and parabolic elements are provided for two- and three-dimensional calculations. In the near future, all the elements of the flux representation will be available. The numerical data for the cross sections are used under the NEPLIB format; they are automatically generated by the APOLLO module of NEPTUNE.

V.B. Numerical Tests

Three numerical comparisons are presented: The first two are designed to measure the accuracy of the method, and the last one is presented as the treatment of a model pressurized water reactor (PWR).

V.B.1. One-Dimensional Test

A reflected slab reactor is considered; the half-thickness of the core is 1 m, and the size of the water reflector is 0.20 m. The core is made of a PWR-like fuel, its enrichment is 2.8%; two-group cross sections were tabulated between 0 and 16 000 MWd/t using APOLLO.

Using piecewise constant cross sections, a standard reference calculation has been performed. The half-reactor is divided into 48 parabolic elements, and the thickness of each element is 0.025 m. Nine diffusion calculations are performed. A depletion step is conducted after each diffusion calculation. The core-averaged irradiation added is 1584 MWd/t.

A second standard calculation is also performed using eight Lagrangian cubic elements, with their boundaries at 0, 0.20, 0.40, 0.60, 0.80, 0.95, 1.00, 1.05, and 1.20 m. The depletion calculation is the same as for the reference calculation.

The third calculation is based on the method presented in this report; the flux representation is based on the same mesh grid as for the second calculation, but the cross sections are represented by linear functions over the eight elements.

The variation of the effective multiplication factor during the depletion calculation is given in Table I. For the first calculation, the cross sections are piecewise constant. Therefore, the two cubic calculations give exactly the same result. Moreover, the coarse-mesh grid used in the cubic calculation seems to be adequate.

During the depletion process, the discrepancy between the standard cubic calculation and the reference calculation increases. It is due to the piecewise constant cross sections. The third result was obtained using the method proposed in this paper. The linear representation of the cross sections almost cancels this discrepancy.

Figures 1 and 2 present the pointwise spatial variation of the thermal fluxes, respectively, at steps 1 and 9. These curves are obtained using the reference calculation data. The difference between the reference thermal flux and the thermal flux obtained with the coarse calculation for the first step is plotted in Fig. 3.

At step 9, three thermal fluxes are obtained, the first using the reference calculation, the second using the standard cubic calculation, and the third using the linear cubic calculation. The errors due to the second and third calculations are plotted in Fig. 4.

The results plotted on Fig. 3 show that the

TABLE I

Variation of the Effective Multiplication Factor of the Slab Reactor During the Depletion

Step	Mean Irradiation (MWd/t)	Reference Calculation	Standard Cubic Calculation	Error ($\times 10^5$)	Linear Cubic Calculation	Error ($\times 10^5$)
1	0	1.27292	1.27290	-2	1.27290	-2
2	1 584	1.24456	1.24470	+14	1.24459	+3
3	3 168	1.22256	1.22276	+20	1.22257	+1
4	4 752	1.20073	1.20101	+28	1.20075	+2
5	6 336	1.18000	1.18032	+32	1.18001	+1
6	7 920	1.16043	1.16079	+36	1.16043	0
7	9 504	1.14194	1.14233	+39	1.14194	0
8	11 088	1.12447	1.12486	+39	1.12444	-3
9	12 672	1.10780	1.10821	+41	1.10775	-5

discrepancy between the coarse cubic calculation and the reference result is lower than 0.1%. The simple representation provides accurate results at the first step.

As shown in Fig. 4, the standard cubic calculation gives errors of ~1%, while the error due to the linear cubic calculation is lower than 0.2%. For this simple case, the finite element method using space-dependent cross sections considerably improves the accuracy of the calculation.

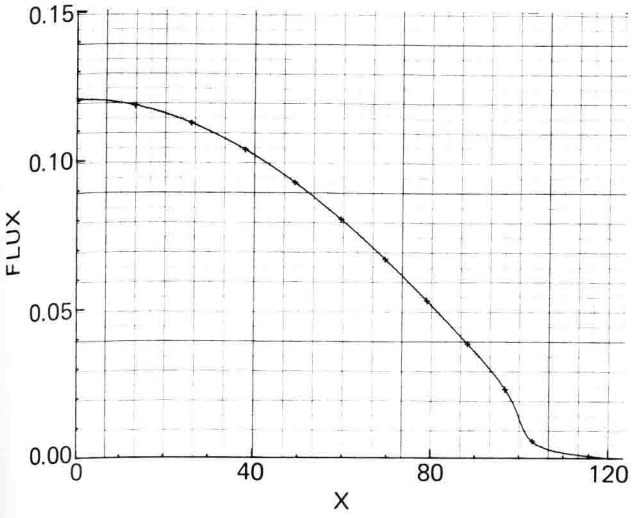

Fig. 1. Step 1 reference thermal flux for the slab reactor.

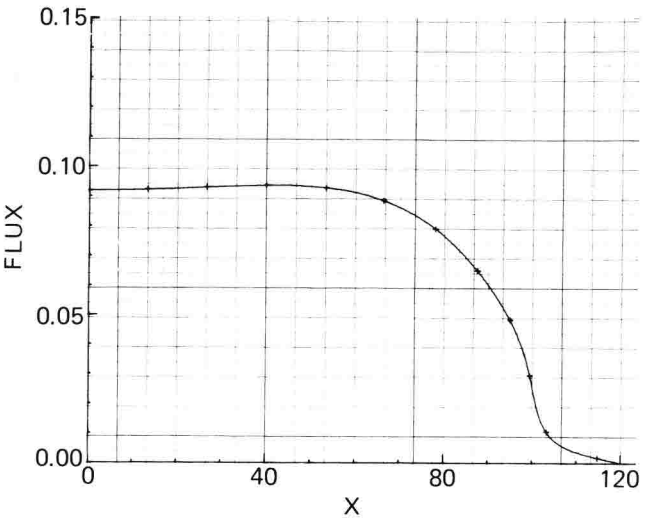

Fig. 2. Step 9 reference thermal flux for the slab reactor.

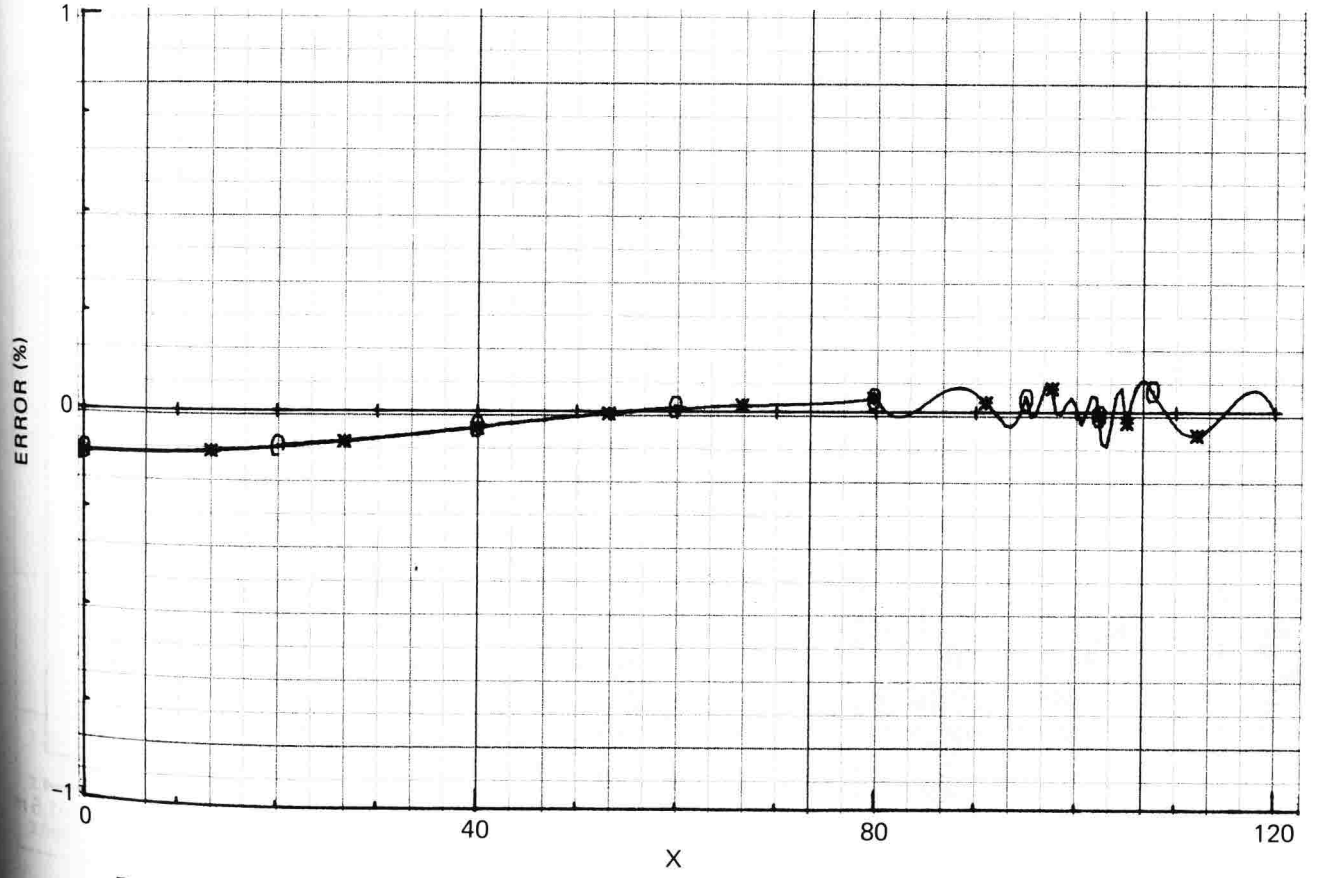

Fig. 3. Difference between the standard cubic thermal flux and the reference flux (step 1 for the slab reactor).

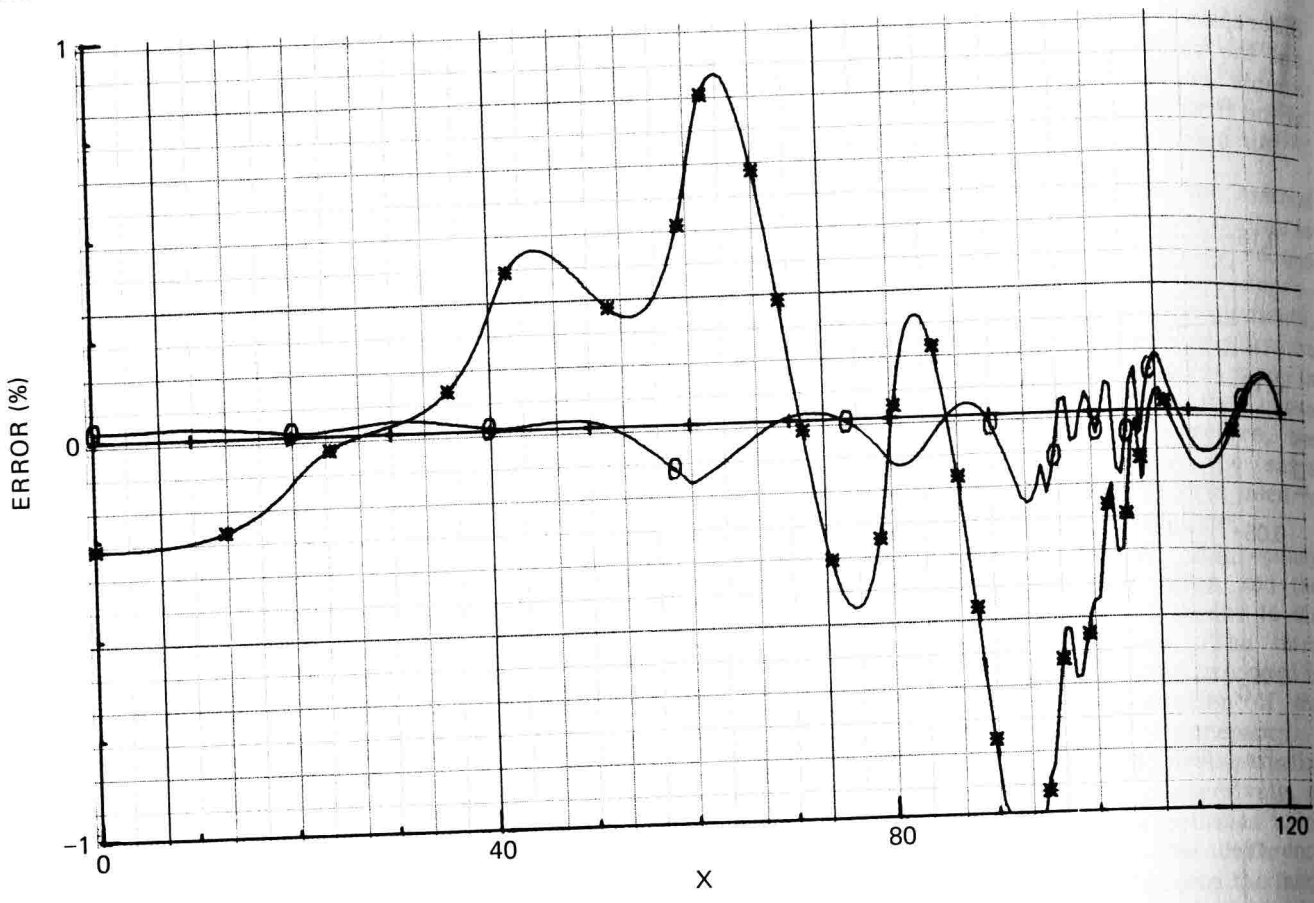

Fig. 4. Difference among the standard cubic thermal flux, the linear cubic thermal flux, and the reference flux (step 9 for the slab reactor). Here, * corresponds to the error due to standard cubic, and 0 corresponds to the error due to linear cubic.

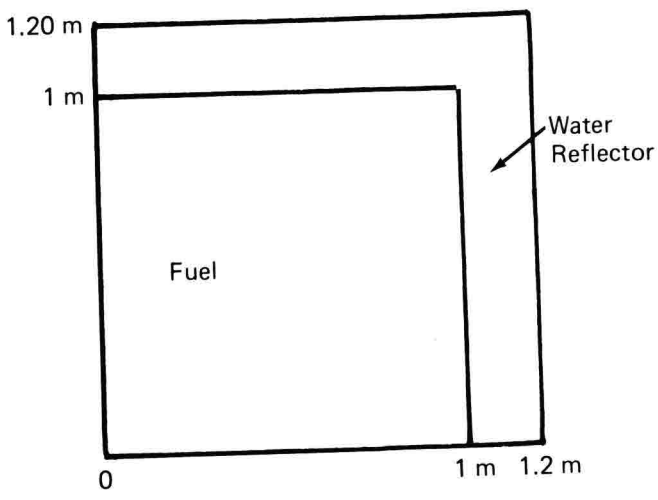

Fig. 5. Homogeneous two-dimensional reactor.

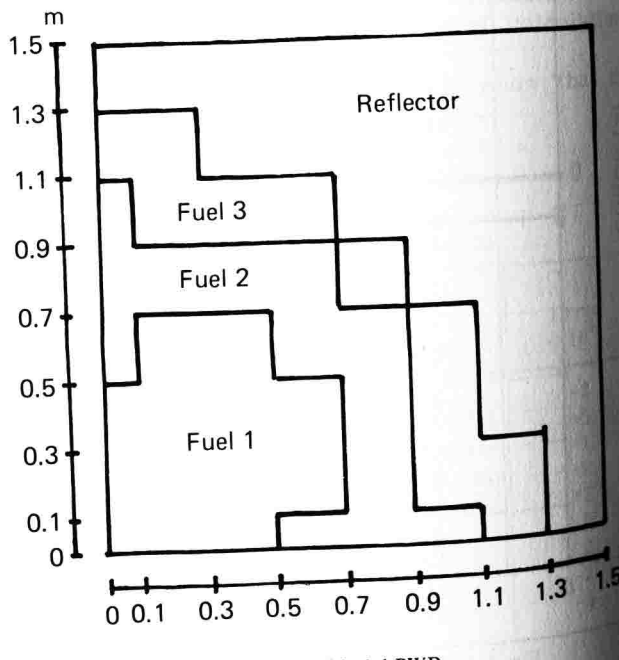

Fig. 6. Model PWR.

TABLE II

Variation of the Effective Multiplication Factor for the Homogeneous Two-Dimensional Reactor

Step	Mean Irradiation (MWd/t)	Reference Calculation	Standard Cubic Calculation	Error ($\times 10^5$)	Linear Cubic Calculation	Error ($\times 10^5$)
1	0	1.25988	1.25987	-1	1.25987	-1
2	1584	1.22744	1.22772	+28	1.22739	-5
3	3168	1.20237	1.20291	+54	1.20231	-6
4	4752	1.17902	1.17980	+78	1.17893	-9
5	6336	1.15746	1.15948	+102	1.15734	-12
6	7920	1.13743	1.13868	+125	1.13726	-17
7	9504	1.11870	1.12015	+145	1.11849	-21

TABLE III

Comparison of the Assembly-Averaged Power Density for the Homogeneous Two-Dimensional Reactor

(Step 1: R = reference result, SC = standard cubic, LC = linear cubic.)

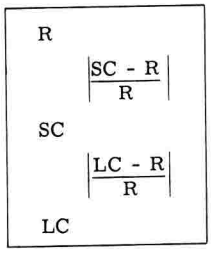

				0.1720 0.41% 0.1713 0.41% 0.1713
			0.6152 0.02% 0.6153 0.02% 0.6153	0.3249 0.2% 0.3242 0.2% 0.3242
		1.180 0% 1.180 0% 1.180	0.8518 0.02% 0.8520 0.02% 0.8520	0.4498 0.22% 0.4488 0.22% 0.4488
	1.694 0.06% 1.695 0.06% 1.695	1.414 0% 1.414 0% 1.414	1.021 0% 1.021 0% 1.021	0.5390 0.20% 0.5379 0.20% 0.5379
1.999 0.05% 2.000 0.05% 2.000	1.840 0.05% 1.841 0.05% 1.841	1.536 0% 1.536 0% 1.536	1.109 0% 1.109 0% 1.109	0.5856 0.22% 0.5843 0.22% 0.5843

TABLE IV

Comparison of the Assembly-Averaged Power Density for the Homogeneous Two-Dimensional Reactor

(Step 7: R = reference result, SC = standard cubic, LC = linear cubic.)

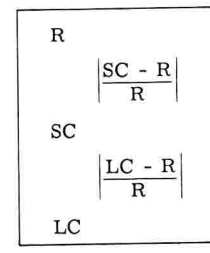

				0.4164 0.02% 0.4165 0.29% 0.4152
			1.008 0.69% 1.015 0.10% 1.007	0.6594 0.44% 0.6623 0.18% 0.6582
		1.221 0.16% 1.223 0% 1.221	1.119 0.54% 1.125 0.09% 1.118	0.7511 0.32% 0.7535 0.20% 0.7496
	1.220 0.49% 1.214 0.16% 1.222	1.224 0.08% 1.223 0.08% 1.225	1.134 0.35% 1.138 0% 1.134	0.7722 0.14% 0.7733 0.18% 0.7708
1.186 0.01% 1.174 0.17% 1.188	1.204 0.75% 1.195 0.17% 1.206	1.211 0.25% 1.208 0.16% 1.213	1.127 0.18% 1.129 0.09% 1.128	0.7722 0.01% 0.7723 0.15% 0.7710

TABLE V

Variation of the Critical Boron Concentration for the Model PWR During the Depletion

Step	Mean Irradiation (MWd/t)	Reference Calculation ($\times 10^4$)	Standard Cubic Calculation	Error ($\times 10^3$)	Linear Cubic Calculation	Error ($\times 10^3$)
1	0	0.4790	0.4787	-0.62	0.4787	-0.62
2	122	0.4714	0.4711	-0.64	0.4710	-0.85
3	612	0.4580	0.4578	-0.44	0.4576	-0.87
4	1593	0.4435	0.4435	0	0.4431	-0.90
5	3554	0.4007	0.4013	+1.50	0.4003	-1.00
6	5515	0.3504	0.3515	+3.14	0.3498	-1.70
7	7477	0.2995	0.3012	+5.70	0.2987	-2.67
8	9438	0.2501	0.2524	+9.20	0.2492	-3.60

TABLE VI

Comparison of the Assembly-Averaged Power Density for the Model PWR

(Step 1: R = reference result, SC = standard cubic, LC = linear cubic.)

R

$\left|\frac{SC - R}{R}\right|$

SC

$\left|\frac{LC - R}{R}\right|$

LC

				0.5649 0.97% 0.5594 0.97% 0.5594		
			1.082 0.09% 1.083 0.09% 1.083	0.8713 0.25% 0.8691 0.25% 0.8691	0.5244 1.10% 0.5186 1.10% 0.5186	
		1.131 0.35% 1.135 0.35% 1.135	1.115 0.18% 1.117 0.18% 1.117	1.102 0.09% 1.103 0.09% 1.103	0.8154 0.58% 0.8106 0.58% 0.8106	
	1.131 0.53% 1.137 0.53% 1.137	1.154 0.43% 1.159 0.43% 1.159	1.199 0.25% 1.202 0.25% 1.202	1.264 0.08% 1.265 0.08% 1.265	1.074 0.18% 1.072 0.18% 1.072	0.5492 1.2% 0.5425 1.2% 0.5425
1.116 0.63% 1.123 0.63% 1.123	1.127 0.62% 1.134 0.62% 1.134	1.173 0.43% 1.178 0.43% 1.178	1.330 0.38% 1.335 0.38% 1.335	1.328 0.08% 1.329 0.08% 1.329	1.103 0.18% 1.101 0.18% 1.101	0.6644 0.68% 0.6599 0.68% 0.6599

V.B.2. A Homogeneous Two-Dimensional Reactor

A simple two-dimensional reactor is considered. A quarter of this reactor is shown in Fig. 5. The fuel and the reflector are the same as in the previous example.

Using piecewise constant cross sections, a standard reference calculation has been performed. Square parabolic elements measuring 0.05×0.05 m are used. Seven diffusion calculations are carried out. A depletion step is performed after each diffusion calculation. The core-averaged irradiation added is 1584 MWd/t.

As in the previous example, a second standard calculation is also carried out using seven Lagrangian cubic elements in each axis, with limits of 0, 0.20, 0.40, 0.60, 0.80, 1.00, 1.10, and 1.20 m. A third calculation is performed on the same mesh grid using a linear representation of the cross sections over each element.

The variation of the effective multiplication factor during depletion is given in Table II. The assembly-averaged power densities are compared in Tables III and IV for steps 1 and 7, respectively. At the first step, the mean square deviation between the reference result and the coarse cubic calculation is equal to 0.15%. At step 7, it

TABLE VII

Comparison of the Assembly-Averaged Power Density for the Model PWR

(Step 6: R = reference result, SC = standard cubic, LC = linear cubic.)

R
$\left\lvert \frac{SC - R}{R} \right\rvert$
SC
$\left\lvert \frac{LC - R}{R} \right\rvert$
LC

				0.6431 0.61% 0.6392 0.65% 0.6389		
			1.117 0.27% 1.120 0.18% 1.119	0.9412 0.20% 0.9431 0.04% 0.9408	0.5897 0.58% 0.5863 0.71% 0.5855	
		1.120 0.36% 1.116 0.27% 1.123	1.116 0% 1.116 0.18% 1.118	1.112 0.45% 1.117 0.09% 1.113	0.8544 0.16% 0.8558 0.34% 0.8515	
	1.111 0.9% 1.101 0.27% 1.114	1.125 0.62% 1.118 0.27% 1.128	1.150 0.09% 1.149 0.17% 1.152	1.201 0.50% 1.207 0.17% 1.203	1.064 0.75% 1.072 0% 1.064	0.5896 0.22% 0.5883 0.88% 0.5844
1.104 1.18% 1.091 0.18% 1.106	1.109 1.0% 1.098 0.18% 1.111	1.131 0.62% 1.124 0.26% 1.134	1.235 0% 1.235 0.24% 1.238	1.233 0.49% 1.239 0.08% 1.234	1.081 0.83% 1.090 0.09% 1.080	0.7057 0.55% 0.7096 0.38% 0.7030

is equal to 0.46% for the standard cubic calculation and to 0.15% for the linear cubic calculation.

For this second example, the conclusions appear to be clear. At the beginning of the calculation, the cubic calculation provides accurate results. For standard calculation, the error increases during the depletion process. This error can be eliminated by use of the linear representation of the cross sections.

V.B.3. A Two-Dimensional Model Reactor

The last example is a model of a PWR. A quarter of this reactor is shown in Fig. 6. There are three different fuel assemblies, the enrichments of which are 2.5, 2.8, and 3.1%, respectively. They are surrounded by a water reflector. The cross sections for these four regions were obtained by APOLLO.

For this example, a determination of the critical boron concentration is performed during the depletion process. A reference calculation is carried out using standard parabolic elements measuring 0.05×0.05 m. There are 30×30 elements.

A second mesh grid is defined using Lagrangian cubic elements measuring 0.20×0.20 m, except for the half-element on the symmetry axis. There

TABLE VIII

Comparison of the Assembly-Averaged Power Density for the Model PWR

(Step 8: R = reference result, SC = standard cubic, LC = linear cubic.)

R	
	$\left\lvert \frac{SC - R}{R} \right\rvert$
SC	
	$\left\lvert \frac{LC - R}{R} \right\rvert$
LC	

				0.6941 0.33% 0.6918 0.70% 0.6892		
			1.125 0.26% 1.128 0.09% 1.126	0.9785 0.48% 0.9832 0.10% 0.9775	0.6367 0.31% 0.6347 0.31% 0.6316	
		1.098 0.64% 1.091 0.27% 1.101	1.103 0.09% 1.102 0.18% 1.105	1.113 0.63% 1.120 0.09% 1.114	0.8849 0.42% 0.8886 0.38% 0.8815	
	1.084 1.38% 1.069 0.28% 1.087	1.095 1% 1.084 0.27% 1.098	1.117 0.36% 1.113 0.18% 1.119	1.171 0.51% 1.177 0.08% 1.172	1.071 1.03% 1.082 0% 1.071	0.6295 0.11% 0.6302 0.9% 0.6238
1.078 1.58% 1.061 0.37% 1.082	1.081 1.39% 1.066 0.37% 1.085	1.096 1.0% 1.085 0.36% 1.100	1.183 0.25% 1.180 0.25% 1.186	1.189 0.50% 1.195 0.17% 1.191	1.082 1.11% 1.094 0% 1.082	0.7484 0.99% 0.7558 0.45% 0.7450

are 8×8 elements. On this mesh grid, two calculations are performed: one with cross sections constant within each assembly (standard cubic) and one with linearly varying cross sections (linear cubic). The critical boron concentration is reported in Table V. The assembly-averaged power densities are compared in Tables VI, VII, and VIII for steps 1, 6, and 8, respectively.

At the first step, the mean square deviation between the reference result and the coarse cubic calculation is equal to 0.55%. For step 6, this deviation is equal to 0.59% for the standard cubic calculation and to 0.35% for the linear cubic calculation. At the last step, the deviation is equal to 0.81% for the standard calculation and to 0.38% for the linear cubic calculation.

For this more realistic case, the finite element method with space-dependent cross sections provides much better accuracy than the standard calculation. During the depletion of the core, the errors in the power density are not larger than at the beginning of the cycle.

The computing time on the IBM System 360/91 for the treatment of one-eighth of the core with Lagrangian cubic elements is ~ 2.23 s. The extra time needed for accounting for space-dependent cross sections is small. Most of the computing time is used for the iteration scheme, which is the same for the two calculations.

VI. CONCLUSION

The new method developed in this report is a finite element treatment of the depletion of a nuclear reactor. Two approximate methods had been developed. The first accounts for space-dependent macroscopic cross sections, while the second is a complete treatment, including any chain of fission products or heavy isotopes. Numerical results have provided several comparisons with standard methods. We expect to carry out more realistic computations, including three-dimensional calculations, to prove the value of this method.

ACKNOWLEDGMENT

The authors are deeply indebted to Mrs. C. Dillet, who performed a large part of the coding and computing work.